$SrAu_{4.76}In_{1.24}$ with $YbMo_2Al_4$-type Structure

Ihor Muts[a,b], Samir F. Matar[c], Ute Ch. Rodewald[b], Vasyl' I. Zaremba[a], and Rainer Pöttgen[b]

[a] Inorganic Chemistry Department, Ivan Franko National University of Lviv, Kyryla and Mephodiya Street 6, 79005 Lviv, Ukraine
[b] Institut für Anorganische und Analytische Chemie, Universität Münster, Corrensstraße 30, 48149 Münster, Germany
[c] CNRS, Université de Bordeaux, ICMCB, 87 Avenue du Docteur Albert Schweitzer, 33600 Pessac, France

Reprint requests to R. Pöttgen. E-mail: pottgen@uni-muenster.de

Z. Naturforsch. **2011**, *66b,* 993 – 999; received September 22, 2011

The gold-rich intermetallic compound $SrAu_{4.76}In_{1.24}$ was synthesized by high-frequence-melting of the elements in a sealed tantalum tube and subsequent annealing. The structure was refined from single-crystal X-ray diffraction data: $YbMo_2Al_4$-type, $I4/mmm$, $Z = 2$, $a = 718.77(7)$, $c = 552.79(9)$ pm, $wR2 = 0.0760$, 149 F^2 values and 11 parameters. The 4*d* (0.62 In + 0.38 Au) Wyckoff position shows mixed occupancy leading to the composition $SrAu_{4.76}In_{1.24}$ for the investigated crystal. The strontium atoms are located in a large cage built up by 12 Au + 8 In atoms. The gold and indium atoms show segregation into substructures. The striking structural motifs are Au_4 squares (278 pm Au–Au) and indium chains (276 pm In–In). The squares and chains are connected *via* weaker Au–Au (299 pm) and Au–In (295 pm) bonds to a three-dimensional network. The In chains show the motif of rod packing. Electronic structure calculations show anisotropy within the structure with different responses to compressions along In–In chains and Au planes, also illustrated by the electron localization contour plots. The metallic behavior is found to be of itinerant electron type (like Cu), and the chemical bonding includes stabilizing Au–In interactions.

Key words: Strontium, Indium, Crystal Structure, Intermetallic Compound

Introduction

The ternary systems alkaline earth metal (*AE*)-gold-indium have intensively been investigated in recent years [1 – 14]. So far 18 compounds have been reported, *i. e.* Ca_3Au_3In [13], isotypic CaAuIn [1] and SrAuIn [11], $CaAuIn_2$ [2], the crystalline approximants $Ca_{14.1}Au_{44.2}In_{41.7}$ and $Ca_3Au_{12.2}In_{6.3}$ [10], $Ca_4Au_{10}In_3$ [8], $Ca_2Au_3In_4$ [3] and $Sr_2Au_3In_4$ [4], the solid solution $SrAu_xIn_{4-x}$ [9], $SrAu_4In_4$ and $Sr_4Au_9In_{13}$ [14], $SrAuIn_3$ [11] and $BaAuIn_3$ [5], $SrAu_3In_3$ [12], $SrAu_2In_2$ and $BaAu_2In_2$ [7], and KHg_2-type $BaAu_{0.36}In_{1.64}$ [6]. Most of these intermetallic compounds have a common structural building principle. The alkaline earth metals transfer electron density to the gold and indium atoms, enabling the covalent bonding within the two- or three-dimensional $[Au_yIn_z]$ polyanionic networks. Besides new structure types, several of the ternary $AE_xAu_yIn_z$ compounds are ordered variants of binary structure types, *e. g.* $Ca_4Au_{10}In_3$ (ordered Zr_7Ni_{10} type), CaAuIn (ordered Co_2Si type), $SrAuIn_3$ (ordered $BaAl_4$ type), or Ca_3Au_3In (ordered Ni_4B_3 type).

In the course of systematic phase analytical studies of the Sr–Au-In system we discovered another gold-rich compound $SrAu_{4.76}In_{1.24}$ which crystallizes with the $YbMo_2Al_4$-type [15] structure. The synthesis and crystal chemistry of $SrAu_{4.76}In_{1.24}$ are reported herein. Further analyses of the electronic band structure and the chemical bonding is provided using computational methods built within the well established quantum theoretical density functional theory (DFT) framework [16, 17].

Experimental Section

Synthesis

Starting materials for the preparation of the $SrAu_{4.76}In_{1.24}$ sample were a strontium rod (Johnson Matthey), pieces of a gold bar (Heraeus), and indium ingots (Johnson Matthey), all with stated purities better than 99.9 %. Pieces of the strontium rod were cut under paraffin oil, washed with *n*-hexane and kept in Schlenk tubes under argon prior to the reactions. The paraffin oil and *n*-hexane were dried over sodium wire. The argon was purified over titanium sponge (900 K), silica gel, and molecular sieves. The elements were weighed

Table 1. Crystallographic data and structure refinement for $SrAu_{4.76}In_{1.24}$.

Empirical formula	$SrAu_{4.76(2)}In_{1.24(2)}$
Molar mass, g mol^{-1}	1167.56
Crystal size, μm^3	$20 \times 20 \times 40$
Space group; Z	$I4/mmm$; 2
Structure type	$YbMo_2Al_4$
Lattice parameters (Guinier powder data)	
a, pm	718.77(7)
c, pm	552.79(9)
Cell volume V, nm^3	0.2856
Calculated density, g cm^{-3}	13.58
Transm. ratio (max / min)	0.777 / 0.363
Radiation	MoK_α
λ, pm	71.073
Absorption coefficient, mm^{-1}	135.8
F(000), e	950
θ range, deg	4 – 31
Range in hkl	±10, ±10, ±7
Total reflections	1627
Independent reflections / R_{int}	149 / 0.1710
Reflections with $I \geq 2\sigma(I)$ / R_σ	146 / 0.0686
Data / parameters	149 / 11
Goodness-of-fit	1.238
$R1$ / $wR2$ for $I \geq 2\sigma(I)$	0.0368 / 0.0756
$R1$ / $wR2$ for all data	0.0374 / 0.0760
Extinction coefficient	0.0041(7)
Largest diff. peak / hole, e Å^{-3}	3.91 / −3.22

in a 1 : 4 : 1 atomic ratio and arc-welded [18] in a tantalum ampoule. The latter was placed in a water-cooled sample chamber [19] of an induction furnace (Hüttinger Elektronik, Freiburg, type TIG 1.5/300) under flowing argon and first annealed at 1400 K for 5 min followed by cooling to 900 K within four hours. Finally the temperature was kept at 900 K for another four hours followed by quenching. The temperature was controlled through a Sensor Therm Methis MS09 pyrometer with an accuracy of ±30 K. The sample was mechanically broken off the tantalum tube. No reaction with the crucible material was evident. The compact polycrystalline sample is stable in air over weeks. Single crystals exhibit metallic lustre while ground powders are light gray.

EDX data

The single crystal investigated on the diffractometer was studied by energy dispersive analyses of X-rays (EDX) using a Zeiss EVO MA10 scanning electron microscope with SrF_2, Au and InAs as standards. The experimentally observed composition (10 ± 2 at-% Sr, 71 ± 2 at-% Au, 19 ± 2 at-% In) was close to the one refined from the X-ray data (14.3 : 68.0 : 17.7), and no impurity elements were observed. The standard uncertainty is due to the irregular surface of the measured crystal (conchoidal fracture).

X-Ray diffraction

The polycrystalline $SrAu_4In$ sample was characterized by a Guinier powder pattern (Cu$K_{\alpha1}$ radiation, α-quartz: a = 491.30, c = 540.46 pm as internal standard). The Guinier camera was equipped with an imaging plate unit (Fuji film, BAS-READER 1800). The tetragonal lattice parameters (Table 1) were obtained from a least-squares fit. Correct assignment of the reflections was ensured by an intensity calculation [20].

Single crystals with conchoidal fracture were selected from the crushed $SrAu_4In$ sample and glued to thin quartz fibres. The crystals were investigated by Laue photographs on a Buerger camera. A data set of a high-quality crystal was collected at r. t. using a STOE IPDS-II image plate system (graphite-monochromatized MoK_α radiation; λ = 71.073 pm) in oscillation mode. A numerical absorption correction was applied to the data set. All relevant crystallographic data are listed in Table 1.

Structure refinement

The data set showed a body-centered tetragonal lattice with high Laue symmetry and no further systematic extinctions, compatible with space group $I4/mmm$. The starting atomic parameters were deduced from Direct Methods with SHELXS-97 [21], and the structure was refined using SHELXL-97 [22] (full-matrix least-squares on F^2) with anisotropic atomic displacement parameters for all sites. The 4*d* site was initially refined with the scattering factor of indium; however, the too small displacement parameter indicated higher electron density on this site. In agreement with the higher gold content measured by EDX, a mixed occupancy In/Au was introduced, and the refinement then smoothly converged to the residuals listed in Table 1 with the composition $SrAu_{4.76}In_{1.24}$ for the investigated crystal. Inspection of the Pearson code tI14 and the Wyckoff sequence 139,hda in the Pearson Crystal Data Base [23] readily revealed isotypism with $YbMo_2Al_4$ [15]. In the final cycles the structure was refined with the setting of the prototype.

Table 2. Atomic coordinates and anisotropic displacement parameters (pm^2) for $SrAu_{4.76}In_{1.24}$. U_{eq} is defined as one third of the trace of the orthogonalized U_{ij} tensor. The anisotropic displacement factor exponent takes the form: $-2\pi^2[(ha^*)^2U_{11} + \cdots + 2hka^*b^*U_{12}]$. $U_{13} = U_{23} = 0$.

Atom	Wyckoff site	x	y	z	$U_{11} = U_{22}$	U_{33}	U_{12}	U_{eq}
Sr	2*a*	0	0	0	143(10)	152(13)	0	146(7)
0.62(2) In + 0.38(2) Au	4*d*	0	1/2	1/4	201(7)	173(8)	0	192(6)
Au	8*h*	0.30649(8)	x	0	149(4)	207(5)	−1(2)	168(4)

Table 3. Interatomic distances (pm) in the structure of $SrAu_{4.76}In_{1.24}$. All distances within the first coordination shells are listed. Standard deviations are all equal or smaller than 0.1 pm. Note that the In site shows mixed occupancy (Table 2).

Sr:	4	Au	311.6	Au:	2	Au	278.2
	8	Au	339.2		4	In	294.9
	8	In	385.0		2	Au	299.3
In:	2	In	276.4		1	Sr	311.6
	8	Au	294.9		2	Sr	339.2
	4	Sr	385.0				

The final difference Fourier synthesis revealed no significant residual peaks (Table 1). The atomic parameters and interatomic distances are listed in Tables 2 and 3.

Further details of the crystal structure investigation may be obtained from Fachinformationszentrum Karlsruhe, 76344 Eggenstein-Leopoldshafen, Germany (fax: +49-7247-808-666; e-mail: crysdata@fiz-karlsruhe.de, http://www.fiz-informationsdienste.de/en/DB/icsd/depot_anforderung.html) on quoting the deposition number CSD-423579.

Computational methodology

Within DFT we use two complementary computational methods. The Vienna *ab initio* simulation package (VASP) code [24] allows geometry optimization and subsequent establishment of the energy-volume equations of states. For this we used ultra soft pseudo potentials [25] built within the local density approximation LDA [26]. Also, despite the overbinding character of the LDA the lattice parameters were computed in better agreement with experiment than using gradient approximation (GGA) potentials [27]. The conjugate-gradient algorithm [28] is used in this computational scheme to relax the atoms. The tetrahedron method with Blöchl corrections [29] as well as a Methfessel-Paxton [30] scheme were applied for both geometry relaxation and total energy calculations. Brillouin zone (BZ) integrals were approximated using the special k-point sampling of Monkhorst and Pack [31]. The optimization of the structural parameters was performed until the forces on the atoms were less than 0.02 eV $Å^{-1}$ and all stress components less than 0.003 eV $Å^{-3}$. The calculations converged at an energy cut-off of 273 eV for the plane-wave basis set with respect to the k-point integration with a starting mesh of $4 \times 4 \times 4$ up to $8 \times 8 \times 8$ for best convergence and relaxation to zero strains. Then all-electron calculations, equally based on the DFT with LDA functional [26], were carried out for a full description of the electronic structure and the properties of chemical bonding. They were performed using the full potential scalar-relativistic augmented spherical wave (ASW) method [32, 33]. In the ASW method, the wave function is expanded in atom-centered augmented spherical waves, which are Hankel functions and numerical solutions of Schrödinger's equation, respectively, outside and inside the so-called augmentation spheres. In the minimal ASW basis set, we chose the outermost shells to represent the valence states, and the matrix elements were constructed using partial waves up to $l_{max} + 1 = 3$ for Sr, In and Au. Self-consistency was achieved when charge transfers and energy changes between two successive cycles were such as: $\Delta Q < 10^{-8}$ and $\Delta E < 10^{-6}$ eV, respectively. The Brillouin zone integrations were performed using the linear tetrahedron method within the irreducible wedge [29]. The calculations were carried out assuming spin degenerate configuration. Besides the site projected density of states, we discuss qualitatively the pair interactions based on the overlap population analysis with the crystal orbital overlap population (COOP) [34]. In the plots, positive, negative, and zero COOP magnitudes indicate bonding, anti-bonding, and non-bonding interactions, respectively. Here we use the integrated iCOOP criterion to address relative bonding intensities. We note that another scheme for describing the chemical bonding, the ECOV (covalent bond energy) criterion based on both the overlap and the Hamiltonian populations, is also accessible within the ASW method [32, 33]. It provides similar qualitative results to the COOP.

Results

Geometry optimization and energy-volume equations of state

Despite the partial occupation of ~ 0.6 In and 0.4 Au on the 4*d* site, we have considered an ordered compound with $SrAu_4In_2$ composition, *i. e.* with a full occupancy of all sites (Table 2). These assumptions are due to the difficulty of accounting for solid solutions within the framework of our calculations. But on the other hand they allow for a relevant analysis

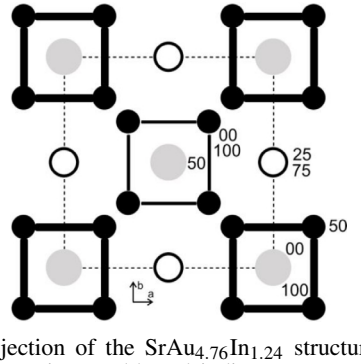

Fig. 1. Projection of the $SrAu_{4.76}In_{1.24}$ structure onto the *xy* plane. Strontium, gold, and indium atoms are drawn as medium grey, black filled, and open circles, respectively. The Au_4 squares and heights of the atoms (in hundredths) are emphasized. Note that the indium position shows mixed occupancy (see Table 2).

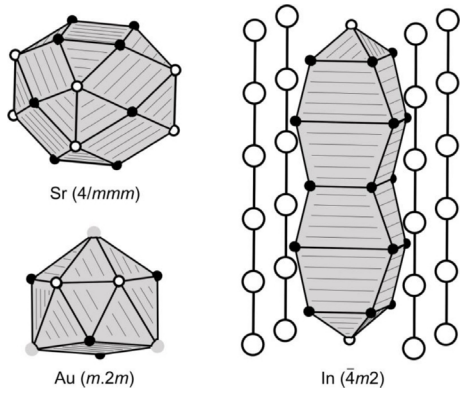

Fig. 2. Coordination polyhedra in the structure of $SrAu_{4.76}In_{1.24}$. Strontium, gold, and indium atoms are drawn as medium grey, black filled, and open circles, respectively. The site symmetries are indicated.

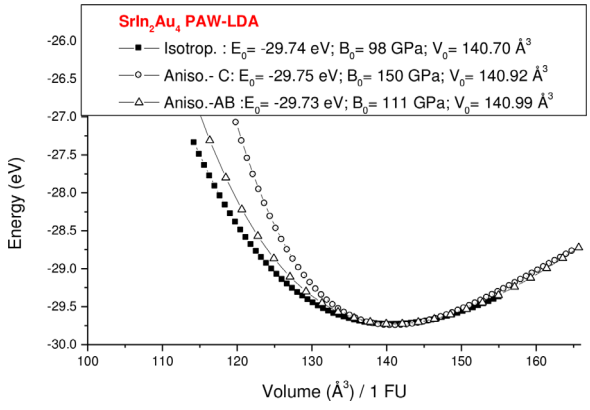

Fig. 3. Energy volume curves for $SrAu_4In_2$ under isotropic and anisotropic compressions with fit values in the insert from Birch equations of state (see text).

of the essentials of the electronic structure and the chemical bonding. Further, we address features relative to the anisotropic crystal structure as shown in Figs. 1 and 2. The optimization of the lattice parameters and the atomic positions determined from single-crystal X-ray data have provided a fairly good agreement with experiment (*cf.* Tables 1 and 2), despite the imposed occupancy, with the following computed data: a = 708, c = 562 pm and x_{Au} = 0.304. Then we calculated the energy-volume equations of states (EOS) of the ordered compound for three configurations pertaining to the anisotropy of the crystal structure (Fig. 2), *i. e.* a (homogeneous) isotropic compression and two anisotropic compressions along the c axis, to evaluate the role of the In–In chains, and along the a,b basal plane to evaluate the role of the square Au–Au substructure. Establishing the energy-volume EOS's improves the geometry optimization procedure. Because the zero of energy depends on the choice of the potentials, somehow it becomes arbitrary; *i. e.* it is shifted but not scaled. However, the energy derivatives as well as the EOS remain unaltered. For this reason one needs to establish the EOS and extract the fit parameters for an assessment of the equilibrium values. This is done from a (E,V) set of calculations around minima found from geometry optimization. The resulting E = f(V) curves are shown in Fig. 3. All three curves have a quadratic variation which can be fitted with an energy-volume Birch EOS to the 3rd order [35]:

$$E(V) = E_o(V_o) + [9/8]V_oB_o\left[([(V_o)/V])^{[2/3]} - 1\right]^2 + [9/16]B_o(B' - 4)V_o\left[([(V_o)/V])^{[2/3]} - 1\right]^3,$$

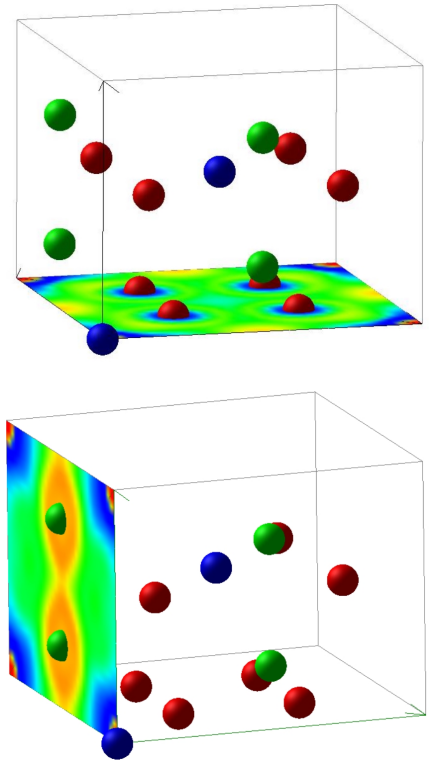

Fig. 4 (color online). Electron localization function (ELF) plots for $SrAu_4In_2$ showing the basal plane containing 4 Au (red spheres) at the top and the vertical plane containing In (green spheres) and Sr (blue spheres) at the bottom. Blue, green and red areas designate weak, free electron-like and strong localizations, respectively (see text).

where E_o, V_o, B_o, and B' are the equilibrium energy, the volume, the bulk modulus, and its pressure deriva-

tive, respectively. Despite their crossing at closely the same minima of energy (E_0) and volume (V_0), the three curves have different shapes pertaining to different bulk moduli B_0. The isotropic compression exhibits the smallest B_0 = 98 GPa with respect to the two anisotropic compressions. The largest B_0 value is obtained for the compression along the *c* axis which aligns the In–In chains (*cf.* Fig. 2) with B_0 = 150 GPa, whereas the other anisotropic compression involving the *a*,*b* plane gives a smaller B_0 = 111 GPa. The pressure derivative B' is close to 4 for both phases, a value usually encountered [36]. The anisotropic compression should also become evident from the electronic localization point of view. This is illustrated by the electron localization function ELF [37] obtained from real space calculations ELF = $(1+\chi_\sigma{}^2)^{-1}$. In this expression the ratio $\chi_\sigma = D_\sigma/D_\sigma{}^\circ$ where $D_\sigma = \tau_\sigma - \nabla s - 1/4(\nabla\rho_\sigma)^2/\rho_\sigma$ and $D_\sigma{}^\circ = 3/5(6\pi^2)^{2/3}\rho_\sigma{}^{5/3}$ correspond respectively to a measure of Pauli repulsion (D_σ) of the actual system and to the free electron gas repulsion ($D_\sigma{}^\circ$) and τ_σ is the kinetic energy density. The ELF function is normalized between 0 (zero localization, blue areas) and 1 (strong localization, red areas) with the value of 1/2 corresponding to a free electron gas behavior. Fig. 4 shows two ELF contour plots for the basal plane containing Au and a vertical plane comprising an In–In chain. Whereas there is a nearly free electron like behavior (green) in the basal plane, some localization (yellow-orange) is identified along the In–In chain. This stronger electron localization along the In–In chain could be the origin of the larger bulk module along the *c* axis. As expected, blue areas of weak localization identify the neighborhood of Sr which is fully (positively) ionized. Nevertheless, the compound exhibits a metallic behavior through the free electron-like smearing as shown by the green areas in both ELF slices. The changes in the electronic structure and derived properties such as the chemical bonding are further discussed in the next sections.

Crystal chemistry

The intermetallic compound $SrAu_{4.76}In_{1.24}$ crystallizes with the tetragonal $YbMo_2Al_4$-type structure [15], space group $I4/mmm$. Besides the prototype, $GdMo_2Al_4$ and $ErMo_2Al_4$ [15], the gallides RTi_2Ga_4 (R = Zr, Sc, Y, Tb, Dy, Ho, Er, Tm, Lu) [38–42] and RV_2Ga_4 (R = Sc, Zr, Er, Hf) [38], also some transition metal-rich compounds $YbCu_{5.1}Al_{0.9}$ [43], $YbCu_{5.12}Al_{0.88}$ [44], and $CeCu_{4.7}Mn_{1.3}$ [45] have been reported. A projection of the $SrAu_{4.76}In_{1.24}$ structure onto the *xy* plane is presented in Fig. 1. The structure contains two striking structural motifs which are directly related to short Au–Au and In–In distances. Each strontium atom is coordinated to two Au_4 squares above and below (Figs. 1 and 2) at Au–Au distances of 278 pm, even slightly shorter than in *fcc* gold (288 pm) [46], indicating substantial Au–Au bonding. These Au_4 squares are connected to a three-dimensional network with weaker (secondary) Au–Au inter-square bonding (299 pm Au–Au). The space between the networks of Au_4 squares is filled by infinite indium chains which extend in the *z* direction. The In–In distances of 276 pm are significantly shorter than the shortest In–In distance of 325 pm in tetragonal body-centered indium [46]. Similar infinite indium chains have been observed in binary Ti_2In_5 [47] and Hf_2In_5 [48], however, with longer In–In distances of 300 and 306 pm, respectively.

Each indium atom within a chain has a slightly distorted, bicapped, square prismatic coordination. Eight gold atoms at 295 pm Au–In build up the square prisms, which are capped by the neighboring indium atoms. The Au–In distances of 295 pm are only slightly longer than the sum of the covalent radii of 284 pm [49]. Such Au–In distances are typically observed in ternary indides of the alkaline earth [1 – 14] and rare earth [50, 51] metals.

The strontium atoms have the high coordination number 20, formed by 12 Au + 8 In atoms. Considering the course of the Pauling electronegativities, 0.95 for Sr, 2.54 for Au, and 1.78 for In, it is clear that one observes closer Sr–Au bonding (312 – 339 pm), as compared to Sr–In (385 pm). The Sr–Au distances compare well with the sum of the covalent radii (326 pm) [49]. Similar ranges have been observed in $Sr_2Au_3In_4$ (308 – 355 pm) [4], $SrAu_3In_3$ (337 pm) [12], $Sr_4Au_9In_{13}$ (343 – 352 pm) [14], and SrAuIn (323 – 330 pm) [11]. Within the $SrAu_{18}$ polyhedron of binary $SrAu_5$ [52], the Sr–Au distances range from 325 to 364 pm. In the structures of $SrAu_4In_4$, $Sr_4Au_9In_{13}$ [14], and $SrAu_5$ [52], the strontium polyhedra derive from pentagonal or hexagonal prisms. The Au_4 squares capping the strontium atoms in $SrAu_{4.76}In_{1.24}$ lead to a different geometry.

A striking feature in many of the $Sr_xAu_yIn_z$ indides is the Au–In mixing within the polyanionic network. Similar to $SrAu_{3.76}In_{4.24}$ [14], $Sr_2Au_{2.85}In_{4.15}$ [4], the broad solid solution $SrAu_xIn_{4-x}$ ($0.5 \leq x \leq 1.2$) [9],

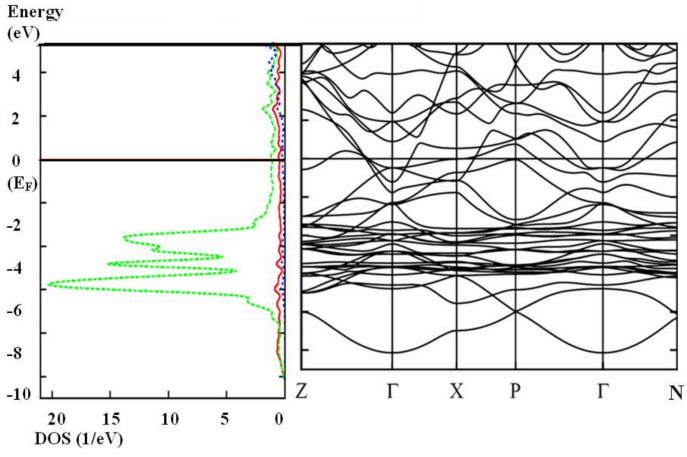

Fig. 5 (color online). Site projected density of states of $SrAu_4In_2$ and mirroring of the band structure along major directions of the Brillouin zone of the body-centered tetragonal lattice. Green, red and blue lines are relevant to the Au, In and Sr PDOS, respectively.

and $SrAuIn_3$ [11], also $SrAu_{4.76}In_{1.24}$ shows Au–In mixing towards the gold-rich region. This Au–In mixing certainly influences the indium chains and leads to a shortening of the distances.

Finally we draw back to the comparison of $SrAu_{4.76}In_{1.24}$ with the prototype $YbMo_2Al_4$ [15]. The coloring of the transition metal and the *p* element (gold takes the aluminum position), however, do not change as a function of the Pauling electronegativity, *i. e.* Mo 2.16 and Al 1.61 *vs.* In 1.78 and Au 2.54 [49]. In view of the different coloring and the differences in chemical bonding we should call the relationship between both structures isopointal [53, 54] rather than isotypic. The chemical bonding peculiarities are addressed in the following section.

Band structure, density of states and chemical bonding

The site projected density of states (PDOS) and the mirroring band structure accounting for site multiplicities are shown in Fig. 5. The energy reference is at the Fermi level (E_F) along the *y* axis. E_F crosses all PDOS at low intensity (dispersive bands). On the opposite nearly full Au *d* states with a sharply localized PDOS within the valence band VB $\{-2, -6$ eV$\}$ are illustrated by flat bands. The lower part of the VB is characterized by highly dispersive bands arising from *s*-like states of In and Au as the similar PDOS shapes suggest. Then the overall behavior of the compound is that of an *s*-like metal such as copper. This is illustrated by the ELF plots showing green free electron-like areas.

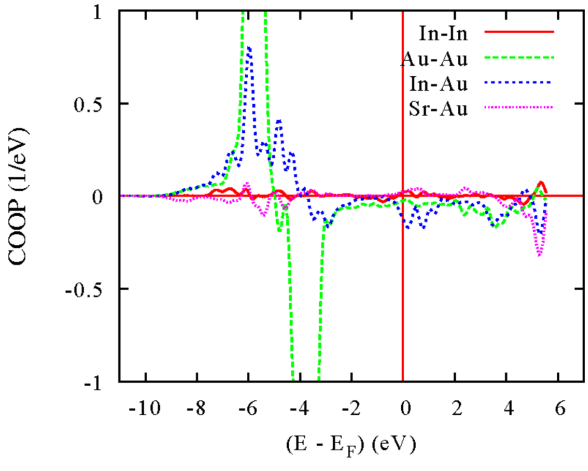

Fig. 6 (color online). Chemical bonding of $SrAu_4In_2$ from a COOP scheme accounting for site multiplicities. For details see text.

The chemical bonding is illustrated in Fig. 6 showing the largest interaction for Au–Au due to the *d* states. Their high filling leads to bonding as well as antibonding COOP intensities which tend to compensate each other (typical closed-shell behavior). On the contrary, the Au–In interactions are mostly bonding, involving Au *d* and In *p* states. Au–In is the most stabilizing interaction for the structure, while In–In and Sr–Au bonding play a minor role as already shown with the ELF.

Acknowledgements

This work was financially supported by the Deutsche Forschungsgemeinschaft. I. M. is indebted to the DAAD for a research fellowship.

[1] D. Kußmann, R.-D. Hoffmann, R. Pöttgen, *Z. Anorg. Allg. Chem*. **1998**, *624*, 1727.
[2] R.-D. Hoffmann, R. Pöttgen, G. A. Landrum, R. Dronskowski, B. Künnen, G. Kotzyba, *Z. Anorg. Allg. Chem*. **1999**, *625*, 789.
[3] R.-D. Hoffmann, R. Pöttgen, *Z. Anorg. Allg. Chem*. **1999**, *625*, 994.
[4] R.-D. Hoffmann, R. Pöttgen, C. Rosenhahn, B. D. Mosel, B. Künnen, G. Kotzyba, *J. Solid State Chem*. **1999**, *145*, 283.
[5] S. Liu, J. D. Corbett, *Inorg. Chem*. **2004**, *43*, 4988.
[6] J.-C. Dai, J. D. Corbett, *Inorg. Chem*. **2006**, *45*, 2104.
[7] J.-C. Dai, J. D. Corbett, *Inorg. Chem*. **2007**, *46*, 4592.
[8] Q. Lin, J. D. Corbett, *Inorg. Chem*. **2007**, *46*, 8722.
[9] A. V. Tkachuk, A. Mar, *J. Solid State Chem*. **2007**, *180*, 2298.
[10] Q. Lin, J. D. Corbett, *J. Am. Chem. Soc*. **2007**, *129*, 6789.
[11] I. R. Muts, R. Pöttgen, V. I. Zaremba, *Z. Anorg. Allg. Chem*. **2007**, *633*, 2591.
[12] I. R. Muts, F. M. Schappacher, W. Hermes, V. I. Zaremba, R. Pöttgen, *J. Solid State Chem*. **2007**, *180*, 2202.
[13] I. R. Muts, V. I. Zaremba, U. Ch. Rodewald, R. Pöttgen, *Z. Anorg. Allg. Chem*. **2008**, *634*, 56.
[14] A. Palasyuk, J.-C. Dai, J. D. Corbett, *Inorg. Chem*. **2008**, *47*, 3128.
[15] M. L. Fornasini, A. Palenzona, *J. Less-Common Met*. **1976**, *45*, 137.
[16] P. Hohenberg, W. Kohn, *Phys. Rev*. **1964**, *136*, B864.
[17] W. Kohn, L. J. Sham, *Phys. Rev*. **1965**, *140*, A1133.
[18] R. Pöttgen, Th. Gulden, A. Simon, *GIT Labor-Fachzeitschrift* **1999**, *43*, 133.
[19] R. Pöttgen, A. Lang, R.-D. Hoffmann, B. Künnen, G. Kotzyba, R. Müllmann, B. D. Mosel, C. Rosenhahn, *Z. Kristallogr*. **1999**, *214*, 143.
[20] K. Yvon, W. Jeitschko, E. Parthé, *J. Appl. Crystallogr.* **1977**, *10*, 73.
[21] G. M. Sheldrick, SHELXS-97, Program for the Solution of Crystal Structures, University of Göttingen, Göttingen (Germany) **1997**. See also: G. M. Sheldrick, *Acta Crystallogr*. **1990**, *A46*, 467.
[22] G. M. Sheldrick, SHELXL-97, Program for the Refinement of Crystal Structures, University of Göttingen, Göttingen (Germany) **1997**. See also: G. M. Sheldrick, *Acta Crystallogr.* **2008**, *A64*, 112.
[23] P. Villars, K. Cenzual, *Pearson's Crystal Data: Crystal Structure Database for Inorganic Compounds* (release 2009/10), ASM International®, Materials Park, Ohio (USA) **2010**.
[24] G. Kresse, J. Furthmüller, *Phys. Rev. B* **1996**, *54*, 11169.
[25] D. Vanderbilt, *Phys. Rev. B* **1990**, *41*, 7892.
[26] S. H. Vosko, L. Wilk, M. Nusair, *Can. J. Phys*. **1980**, *58*, 1200.
[27] J. Perdew, K. Burke, M. Ernzerhof, *Phys. Rev. Lett*. **1996**, *77*, 3865.
[28] W. H. Press, B. P. Flannery, S. A. Teukolsky, W. T. Vetterling, *Numerical Recipes*, Cambridge University Press, New York, **1986**.
[29] P. E. Blöchl, *Phys. Rev. B* **1994**, *50*, 17953.
[30] M. Methfessel, A. T. Paxton, *Phys. Rev. B* **1989**, *40*, 3616.
[31] H. J. Monkhorst, J. D. Pack, *Phys. Rev. B* **1976**, *13*, 5188.
[32] A. R. Williams, J. Kübler, C. D. Gelatt, *Phys. Rev. B* **1979**, *19*, 6094.
[33] V. Eyert, *The Augmented Spherical Wave Method – A Comprehensive Treatment*, Lecture Notes in Physics, Springer, Heidelberg, **2007**.
[34] R. Hoffmann, *Angew. Chem*. **1987**, *99*, 871; *Angew. Chem., Int. Ed. Engl*. **1987**, *26*, 846.
[35] F. Birch, *J. Geophys. Res*. **1978**, *83*, 1257.
[36] S. F. Matar, G. Demazeau, M. H. Möller, R. Pöttgen, *Chem. Phys. Lett*. **2011**, *508*, 21.
[37] A. D. Becke, K. E. Edgecomb, *J. Chem. Phys*. **1990**, *92*, 5397.
[38] Y. Grin, I. S. Gavrilenko, V. Y. Markiv, Y. P. Yarmolyuk, *Dopov. Akad. Nauk Ukr. RSR, Ser. A* **1980**, 73.
[39] V. Y. Markiv, *Dopov. Akad. Nauk Ukr. RSR, Ser. A* **1981**, 4.
[40] V. Y. Markiv, T. G. Zhunkivska, N. M. Velyavina, O. O. Lisenko, *Dopov. Akad. Nauk Ukr. RSR, Ser. A* **1983**, 5.
[41] K. Gosh, S. Ramakrishnan, G. Chandra, *J. Magn. Magn. Mater*. **1993**, *119*, L5.
[42] H. Abe, K. Yoshii, H. Kitazawa, *J. Phys. Soc. Jpn*. **2001**, *70*, 3042.
[43] B. M. Stel'makhovych, Y. B. Kuz'ma, L. G. Akselrud, *Russ. Metall*. **1993**, *1*, 173.
[44] B. M. Stel'makhovych, Y. B. Kuz'ma, V. S. Babizhet'sky, *J. Alloys Compd*. **1993**, *190*, 161.
[45] P. Manfrinetti, M. L. Fornasini, D. Mazzone, S. K. Dhar, R. Kulkarni, *J. Alloys Compd*. **2004**, *379*, 64.
[46] J. Donohue, *The Structures of the Elements,* Wiley, New York **1974**.
[47] R. Pöttgen, *Z. Naturforsch*. **1995**, *50b*, 1505.
[48] R. Pöttgen, R. Dronskowski, *Chem. Eur. J*. **1996**, *2*, 800.
[49] J. Emsley, *The Elements*, Oxford University Press, Oxford **1999**.
[50] R.-D. Hoffmann, R. Pöttgen, V. I. Zaremba, Ya. M. Kalychak, *Z. Naturforsch*. **2000**, *55b*, 834.
[51] R. Pöttgen, *J. Mater. Chem*. **1996**, *6*, 63.
[52] M. Feller Kniepmeier, T. Heumann, *Z. Metallkd*. **1960**, *51*, 404.
[53] L. M. Gelato, E. Parthé, *J. Appl. Crystallogr*. **1987**, *20*, 139.
[54] E. Parthé, L. M. Gelato, *Acta Crystallogr*. **1984**, *A40*, 169.